THYROID
Volume 24, Number 2, 2014

DOI: 10.1089/thy.2013.0118

Three-Dimensional Telomere Dynamics in Follicular Thyroid Cancer

Landon Wark,[1,2] Adrian Danescu,[1] Suchitra Natarajan,[1] Xuguang Zhu,[3] Sheue-yann Cheng,[3] Sabine Hombach-Klonisch,[1,4] Sabine Mai,[1,2,5] and Thomas Klonisch[1,6,7]

Background: Over the last decade, annual incidence rates for thyroid cancer have been among the highest of all cancers in the Western world. However, the genomic mechanisms impacting thyroid carcinogenesis remain elusive.
Methods: We employed an established mouse model of follicular thyroid cancer (FTC) with a homozygous proline to valine mutation ($Thrb^{PV/PV}$) in the thyroid receptor β1 (TRβ1) and applied quantitative three-dimensional (3D) telomere analysis to determine 3D telomeric profiles in $Thrb^{PV/PV}$, $Thrb^{PV/+}$, and $Thrb^{+/+}$ mouse thyrocytes before and after histological presentation of FTC.
Results: Using quantitative fluorescent *in situ* hybridization (Q-FISH) and TeloView™ image analysis, we found altered telomeric signatures specifically in mutant mouse thyrocytes. As early as 1 month of age, $Thrb^{PV/PV}$ mouse thyrocytes showed more telomeres than normal and heterozygous age-matched counterparts. Importantly, at the very early age of 1 month, 3D telomeric profiles of $Thrb^{PV/PV}$ thyrocyte nuclei reveal genetic heterogeneity with several nuclei populations exhibiting different telomere numbers, suggestive of various degrees of aneuploidy within the same animal. This was detected exclusively in $Thrb^{PV/PV}$ mice well before the presentation of histological signs of thyroid carcinoma.
Conclusions: We identified quantitative 3D telomere analysis as a novel tool for early detection and monitoring of thyrocyte chromosomal (in)stability. This technique has the potential to identify human patients at risk for developing thyroid carcinoma.

Introduction

Thyroid cancer is the most common carcinoma of endocrine glands and accounts for approximately 1% of all malignancies. For more than a decade now, thyroid cancer has seen one of the highest incidence rates annually of all cancers in the Western world, with 6.1 cases per 100,000 men and 18.2 cases per 100,000 women. These rates represent a sixfold increase since 1975 (1). A combination of more sensitive detection methods and unknown molecular/environmental factors likely contribute to this higher incidence of thyroid cancer (2). Among the three major groups of thyroid cancer—papillary (PTC), follicular (FTC), and undifferentiated (UTC)—PTC is the most common form, accounting for 80% of all thyroid carcinoma, followed by FTC and UTC at approximately 15% and 2% respectively (2). In 3–7% of cases, PTC and FTC occur as part of a hereditary syndrome (3,4), which involves mutations in the *PTEN* gene locus (10q22–23) and inactivating mutations in the gene encoding the regulatory subunit 1A of the cAMP-dependent protein kinase (*PKAR1A*; 2p16, 17q23) resulting in the constitutive activation of protein kinase A (5,6), which has been linked to nonthyroidal tumors in disease states such as Cowden's disease (5). Genetic instability with aneuploidy and allelic loss are common in FTC. Apart from a role for PTEN in FTC (4,7,8), both follicular adenoma and FTC contain mutations in all three RAS genes (*H-RAS, N-RAS, K-RAS*), with a higher prevalence in FTC. RAS mutations rarely coincide with oncogenic PAX8-PPARγ chromosomal 3p25 and 2q13 rearrangement found exclusively in FTC (9) and the inhibition of PPARγ tumor suppressor function contributes to FTC (10,11).

Thyroid hormone receptor β1 (TRβ1) is a nuclear thyroid hormone receptor and is regulated by triiodothyronine (T3). Mutations of TRβ1 have been found in human thyroid cancer (12). In human FTC and the $TR\beta1^{PV}$ mutant mouse model ($Thrb^{PV/PV}$) of FTC, RAS mutations, *PAX8-PPAR*γ rearrangements, and mutations resulting in the activation of the AKT pathway are important contributors to the pathogenesis of

Departments of [1]Human Anatomy & Cell Science, [4]Obstetrics, Gynecology, & Reproductive Medicine, [5]Physiology, [6]Medical Microbiology & Infectious Diseases, and [7]Surgery, Faculty of Medicine, University of Manitoba, Winnipeg, Canada.
[2]Genomic Center for Cancer Research and Diagnosis, Manitoba Institute of Cell Biology, Winnipeg, Canada.
[3]Laboratory of Molecular Biology, National Cancer Institute, National Institutes of Health, Bethesda, Maryland.

FTC (11,13,14). Similar to human FTC, we have shown that homozygous $Thrb^{PV/PV}$ knock-in mice harbor a dominant negative *TRβ1* mutant PV and spontaneously develop FTC and distant metastasis (15). These mice have a human-like thyroid hormone resistance syndrome resulting in the complete loss of T3-binding and transcriptional activation (16). $TR\beta1^{PV/PV}$ homozygous mice have enlarged thyroid glands, are resistant to thyroid hormones, and display high serum thyrotropin (TSH; 400–500-fold increase over normal) and thyroid hormone (9–15-fold increase over normal) levels. $Thrb^{PV/PV}$ homozygotes develop highly invasive and metastasizing FTC in more than 80% of animals at 5–6 months of age, whereas no apparent abnormalities are observed in the wild-type $Thrb^{+/+}$ and heterozygous $Thrb^{PV/+}$ mice.

Telomeres are repetitive nucleotide sequences ($TTAGGG_n$) at the ends of the chromosomes that protect chromosomes from fusions and illegitimate recombination events, as long as they are capped by a protein complex termed "shelterin" (17). The nuclear organization of telomeres in interphase nuclei is directly linked to chromosomal instability (CIN). We showed that deregulation of c-Myc causes telomere remodelling and promotes CIN and carcinogenesis (18,19). A shelterin complex composed of telomeric repeat binding factor (TRF) 1 and 2, and protection of telomeres (POT) 1 proteins directly interact with the TTAGGG repeat of the telomere sequence, and these proteins are interconnected by TPP1, TIN2, and Rap1 (17). Events leading to alterations in this shelterin complex can result in telomeres with impaired protective functions, which cause chromosomal fusions, continuous breakage–fusion–bridge (BFB) cycles, chromosomal imbalances, and gene amplifications. These events will ultimately lead to the generation of complex nonreciprocal translocations, a hallmark of solid tumours and genomic instability in general (20–23). We previously showed significant differences in telomeric profiles (i.e., in telomere signal intensity and number, the presence/absence of telomeric aggregates, and in the number of telomeres per nuclear volumes) in therapy-sensitive and therapy-resistant Hodgkin's lymphoma patients (24). These results demonstrated the prognostic value of three-dimensional (3D) telomere diagnostic imaging for glioblastoma patients (25), and suggested a 3D telomere dysfunction-based progression model leading to the progression of myelodysplastic syndromes to acute myeloid leukemias (26).

In the present study, we applied quantitative 3D telomere imaging techniques to monitor differences in telomere profiles during FTC in thyrocytes of homozygous $Thrb^{PV/PV}$ mice and compared these data to thyroid tissues from heterozygous $Thrb^{PV/+}$ and wild type $Thrb^{+/+}$ mice.

Materials and Methods

Animal work

Animal study protocols were approved by the National Cancer Institute Animal Care and Use Committee. The generation of the $Thrb^{PV/PV}$ mice was described previously (27). Mice harboring the targeted PV mutation are designated as $Thrb^{PV/PV}$ and $Thrb^{PV/+}$ for homozygous and heterozygous mutant mice respectively. Thyroid tissue sections of $Thrb^{+/+}$, $Thrb^{PV/+}$, and $Thrb^{PV/PV}$ animals were investigated for this study. The pathological progression of FTC in $Thrb^{PV/PV}$ mice was described previously (15). At the age of 12.9 months, only 50% of $Thrb^{PV/PV}$ mice were still alive, and 20% of $Thrb^{PV/PV}$ mice survived to the age of 14 months. Histopathologic findings were consistent with FTC progression. Information on animal numbers, sex, and age for each genotype are summarized in Table 1.

Quantitative fluorescent in situ *hybridization*

Q-FISH analysis was performed on 5 μm thick sections of mouse thyroid tissues. Tissue sections were deparaffinized in xylene for 15 min and placed for 1 min in 100% ethanol before a 20 min incubation at 80°C in 1 M sodium thiocyanate to remove RNA and tissue impurities causing autofluorescence before fixation (28). Tissues were postfixed with 10% formaldehyde in 1× phosphate buffer solution (PBS) for 20 min and washed twice for 5 min with PBS. Slides were soaked in 0.5% Triton X-100 for 10 min and transferred for 1 h to 20% glycerol. Thereafter, slides were briefly submerged in liquid nitrogen and allowed to thaw prior to submerging the slides in 20% glycerol. This process was repeated four times and then slides were washed in PBS three times for 5 min. The slides were incubated in 0.1 M HCl with pepsin at a final concentration of 50 μg/mL for 10 min at 37°C. Slides were washed in PBS and stored in 70% deionized formamide/2× standard saline citrate (SSC; pH 7.0), 4°C for at least 1 h. Peptide nucleic acid (PNA) telomere probe (Dako, Mississauga, Canada) was applied to the slides, denatured at 80°C for 3 min, and hybridized at 37°C for 2 h in a Hybrite™ hybridization chamber (Abbott, IL). Once the hybridization was completed, slides were washed twice in 70% formamide/10 mM Tris-HCl (pH 7.4) for 15 min each before being washed for 1 min in 1× PBS, then in 0.1× SSC for 5 min and twice for 5 min each in 2× SSC/0.05% Tween-20. Finally, 0.1 μg/mL DAPI was added to the slides before they were submerged in double-distilled H_2O and dehydrated in a 70%, 90%, 100% ethanol series for 2 min each and coverslipped with Vectashield (Vector Labs Canada, Burlington, Canada).

Image analysis

Using a ZeissAxioImager Z1 microscope with a Zeiss AxioCam HRm digital camera (Zeiss, Jena, Germany), 100 nuclear images per mouse sample were acquired. A rhodamine filter with an exposure time of 500 msec was used to image the cy3 labeled telomere probe with a DAPI chromatin counterstain. Images were taken at 100 focal planes (scale lateral: 0.107 μm/pixel; scale axial: 0.2 μm/slice) for each experiment. Images were deconvolved using a constrained iterative algorithm (29). Intensity analysis was performed with TeloView™ (30,31) with the rhodamine signal intensity providing the relative fluorescent intensities of telomere signals that are proportional to telomere size (32). Cells within the thyroid gland tissue that differed distinctly by their elongated cellular and nuclear shape from normal and

Table 1. Summary of $Thrb^{+/+}$, $Thrb^{PV/+}$, and $Thrb^{PV/PV}$ Mice Used in Q-FISH Experiments

Months	$Thrb^{+/+}$ *(male/female)*	$Thrb^{PV/+}$ *(male/female)*	$Thrb^{PV/PV}$ *(male/female)*
1–4.9	4/2	5/4	8/8
5–12+	10/7	4/6	6/5

carcinogenic thyrocytes were imaged as an internal control (Fig. 1B, white arrows) to confirm that changes in 3D telomeric architecture or signal intensity were not common to all cells in the thyroid tissue but specific to thyrocytes. A/C ratio analysis was performed with TeloView™ (30,31), and the rhodamine signal intensity provided relative fluorescent intensities of telomere signals proportional to telomere size (32). The TeloView™ software calculates the center of gravity and the integrated intensity of each telomere and the latter determines the length of the telomere. Telomere aggregates (TA) are larger than single telomeres, represent telomere clusters that cannot be further resolved by conventional microscopy, and show high-intensity hybridization signals. In all samples studied, we were unable to detect TA using TeloView™ software.

Statistics

p-Values for comparing means were calculated using a two-tailed Student's *t*-test assuming equal variance. Given that we obtained more samples from one genotype than another for most of our age groups, we elected to express the total number of cells with a given number of signals as a percentage of cells within that genotype, as well as the number of signals with a given intensity per 100 cells in order to prevent favoring larger sample sizes.

Results

We performed Q-FISH for the detection of telomeres in interphase nuclei on thyroid tissues of $Thrb^{PV/PV}$, $Thrb^{PV/+}$, and $Thrb^{+/+}$ mice between 1 and 13 months of age (Table 1) followed by quantitative 3D image analysis. Independent of the sex of the animals, the Q-FISH telomere analysis revealed changes in mean telomere signal numbers (Table 2) that were specific to thyrocytes (Fig. 1A, B) but were not observed in other nonfollicular cell populations in the thyroid gland as determined by their interfollicular location and nuclear shape (Fig. 1C, D). Of the expected 160 telomeres of mouse chromosomes (four signals per chromosome), 3D telomere FISH and subsequent quantitative analysis using TeloView detects on average 40 separated telomeres in whole interphase nuclei of cultured cells with complete hybridization efficiency as shown in 2D FISH metaphase spreads (30,31). This number is equivalent to previously published findings (33–35). For our analysis, we did not investigate cultured cells but 5 μm tissue sections. We measured a range for thyrocyte nuclear diameters between 4.5 μm and 10.2 μm in hematoxylin and eosin (H&E) sections, indicating that nuclei in tissue sections are not always complete but represent segments of different nuclear volumes. Our analysis confirmed this situation, as we detected on average 21 telomere signals in thyrocyte nuclei of $Thrb^{+/+}$ controls (Figs. 2A, 3A; Table 2). Thus, we considered nuclear segments in a 5 μm thick section of thyroid tissue having more than 30 telomeric signals as potentially being aneuploid and nuclear segments having more than 40 signals as potentially being near tetraploid or tetraploid. As early as 1 month of age (Fig. 2A–E), thyrocytes in the $Thrb^{PV/PV}$ and $Thrb^{PV/+}$ group showed larger number of telomere signals compared to $Thrb^{+/+}$ thyrocytes (Fig. 2C–E; Table 2). Thyrocytes of the $Thrb^{PV/+}$ and $Thrb^{PV/PV}$ genotypes continued to show a significantly higher average number of telomere signals compared to the $Thrb^{+/+}$ controls for all age groups studied (Table 2). In both mutants, we observed a higher

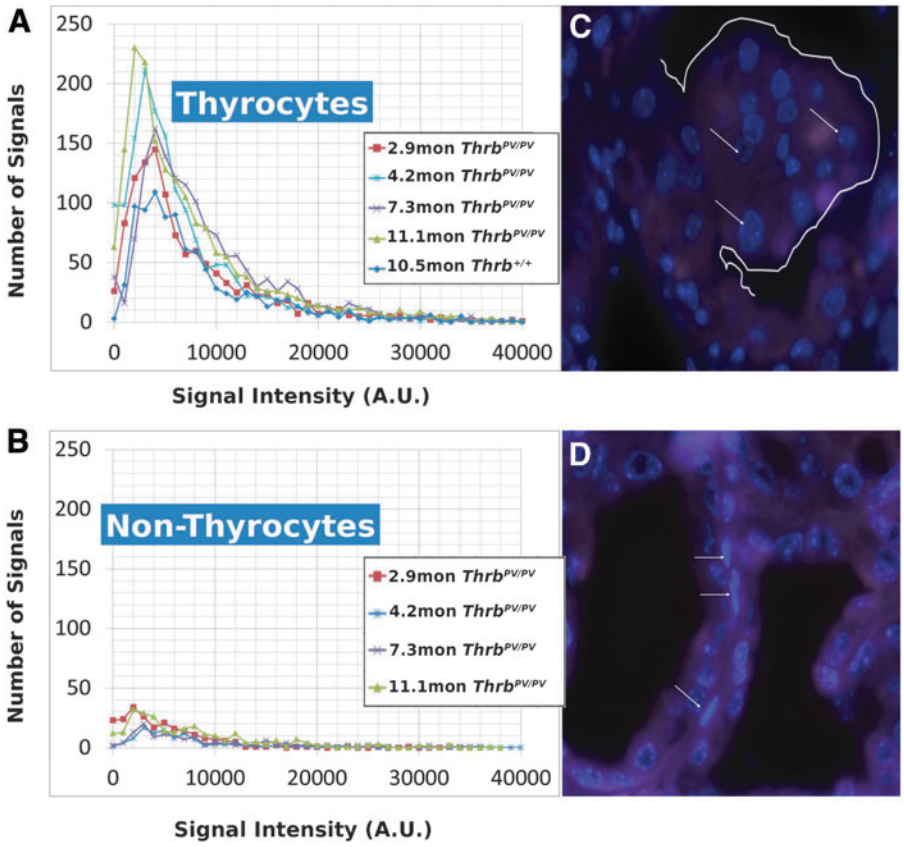

FIG. 1. **(A)** Intensity measurements of $Thrb^{PV/PV}$ thyrocytes at various ages compared with normal and an example area of a polyp (white outline) in a $Thrb^{PV/PV}$ mouse thyroid section **(B)** containing thyrocytes (white arrows). **(C)** Intensity measurements of $Thrb^{PV/PV}$ fibroblasts and an example image in a $Thrb^{PV/PV}$ thyroid **(D**; white arrows**)** used as an internal control for telomere intensity and number.

Table 2. Summary of Mean Number of Signals and Statistical Analysis for All Age Groups

	$Thrb^{+/+}$	$Thrb^{PV/+}$	$Thrb^{PV/PV}$
1–4.9 months			
Mean number of signals	23.5539	28.0067	28.3045
SD	11.2705	11.5752	16.6082
vs. $Thrb^{PV/+}$	$p = 2.09E{-}021$		
vs. $Thrb^{PV/PV}$	$p = 1.37E{-}021$	$p = 0.639$	
5–12+ months			
Mean number of signals	20.4151	26.1780	26.2810
SD	10.2038	8.6749	14.9949
vs. $Thrb^{PV/+}$	$p = 5.90E{-}48$		
vs. $Thrb^{PV/PV}$	$p = 7.71E{-}32$	$p = 0.851$	

SD, standard deviation.

percentage of nuclei showing higher telomere signals than corresponding controls (Figs. 2A, 3A). Intensity measurements of these signals showed that thyrocyte nuclei of homozygous mutants amassed a larger number of low intensity signals, indicative of shorter telomeres (32), than their normal counterparts in the 1–4.9 months age group (Fig. 2B). However, only thyrocyte nuclei of $Thrb^{PV/PV}$ showed a peak in the number of critically short telomeres in the 1–4.9 months age group (Fig. 2A) and continued to have an increased number of short telomeres in the 5–12+ months age group (Fig. 3A). Compared to the controls, the $Thrb^{PV/+}$ heterozygous mice showed an increased number of telomere signals with higher intensities in the 1–4.9 months (Fig. 2A) and the 5–12+ months age group (Fig. 3A).

Data from representative thyroid samples from each genotype for every age group are shown as signal intensity per 100 nuclei (Figs. 2D, 3D) and as the number of nuclei with defined number of telomere signals per 100 thyrocytes (Figs. 2E, 3E). As expected, the graphs in D resembled the curves for the average number of signals analyzed in all samples per age group (Figs. 2B, 3B). When we separated the number of nuclei with defined signal numbers for each animal, $Thrb^{PV/PV}$ mutants revealed a spiked pattern (arrows in Figs. 2E, 3E) resembling several cell populations with different telomere numbers indicative of various degrees of aneuploidy per sample. We observed a small number of cells with more than 80 telomere signals exclusively in $Thrb^{PV/PV}$ thyrocytes at the 1–4.9 months age group (Fig. 2E) and thyrocyte populations showing 50 or more telomere signals per nucleus indicative of the presence of tetraploid thyrocytes. $Thrb^{PV/VP}$ mice at 5–12+ months of age revealed fewer cell populations and reduced number of telomere signals when compared to thyrocytes of $Thrb^{PV/+}$ or controls (Fig. 3E) and the few $Thrb^{PV/PV}$ mice investigated at the age of 12 months and above appeared to have only two populations. None of the $Thrb^{PV/+}$ heterozygous mice or the controls presented a spiked pattern in any of the age groups investigated.

We have previously shown that the spherical nature of telomere distribution (the *a/c* ratio) is associated with the cell cycle phase, with higher ratios indicating more cells at the G2/M boundary and thus a higher overall level of cell proliferation: *a/c* ratios of 1.4 ± 0.1, 1.5 ± 0.2 and 14 ± 2 refer to nuclei in Go/G1, S, and G2 respectively (30,36). Although we determined a higher *a/c* ratio in the $Thrb^{PV/PV}$ and the $Thrb^{PV/+}$, mutants in the 1–4.9 month age group (Supplementary Table S1; Supplementary Data are available online at www.liebert.com/thy), an *a/c* ratio of just over 2.0 fails to indicate the presence of a telomeric disc at G2/M or a higher rate of cell division. However, the analysis of nuclear segments in tissues rather than complete nuclei (as achievable in cultured cells) may limit the informative value of the *a/c* parameter. Since the segmental nuclei we analyzed did not reveal an *a/c* ratio indicative of G2 phase (30), we concluded that more than 40 telomere signals per nucleus reflected near tetraploid or tetraploid thyrocytes.

Discussion

Like other interphase nuclear FISH techniques (37), 3D telomere Q-FISH analysis of interphase nuclei is a highly sensitive method and was used in this study to quantify the length, number of telomeres, presence of TA, and the overall distribution of telomeres (*a/c* ratio) in individual thyroid epithelial cell nuclei in the $Thrb^{PV/PV}$ mouse model of FTC. In the thyroid gland of $Thrb^{PV/PV}$ mice, alterations in 3D nuclear telomere architecture were exclusively observed in thyrocytes and absent in other cell types within the thyroid gland. The latter finding exemplifies a strength of 3D telomere FISH over Southern blot-based terminal restriction fragment assays (TRF), which also measures contamination of surrounding stromal, vascular, or interstitial cells. Similarly, 2D FISH only assesses telomere signals in a single optical plane and requires metaphases reflective of the proliferative cell population only. By contrast, 3D Q-FISH analysis of interphase nuclei assesses telomere signals in every single cell of the population analyzed.

Our 3D telomere FISH analysis revealed, for the first time, changes in telomere number and length as early as 1 month of age in thyrocytes of $Thrb^{PV/PV}$ mice. Similarly, in 2.4 month old $Thrb^{PV/PV}$ mice, the combined use of histopathology and quantitative 3D Q-FISH revealed the presence of an altered telomere architecture and an increased number of critically short telomeres in thyrocyte aggregates protruding into the thyroid follicular lumen (Fig. 1A, B). All $Thrb^{PV/PV}$ mice investigated revealed an increased average number of total telomeres as early as 1–4.9 months of age (Table 2; Fig. 2A) and showed a higher percentage of cells with short telomeres (Fig. 2B). These results suggest early focal appearance of thyrocytes with abnormal telomere phenotypes which may contribute to FTC in the $Thrb^{PV/PV}$ mouse model. Precancerous stages and cancer can both present with telomere shortening (38,39), and FISH-based detection of shorter telomeres in histological specimens was shown to be an early event in human prostate, pancreas, bladder, large intestine, esophagus, oral cavity, and uterine cervix cancer development (39–41). However, shorter telomeres are not always associated with cancer but have also been described in breast ductal carcinoma *in situ* and in normal breast secretory cells (38).

Telomere length is an essential parameter of telomere protective function and maintained in various cell types either by telomerase-dependent or alternative telomere lengthening mechanisms (ALT) (42,43). Telomere length characteristics are species-specific, differ considerably between human and mouse (44,45), between mouse strains (44), and in different tissues of the same mouse strain with age. While brain and spleen mouse tissues develop significant changes in telomere

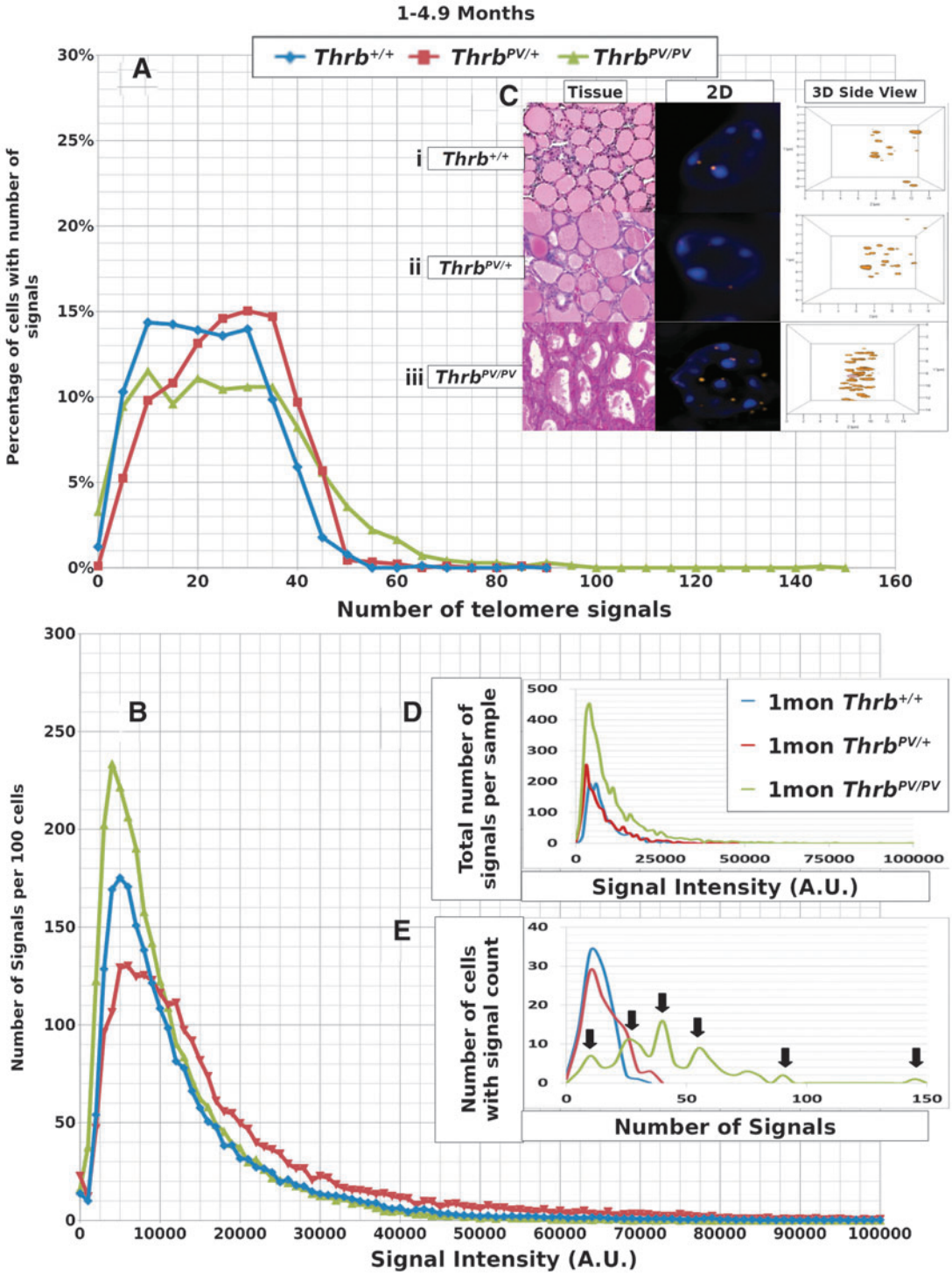

FIG. 2. Data for 1–4.9 month old mouse thyrocytes. **(A)** *y*-Axis indicates the percentage of cells in the given genotypes that have the number of signals shown on the *x*-axis. This percentage was determined by dividing the number of cells with a specific number of signals by the total number of cells observed for each particular genotype. A shift to the right was observed in the $Thrb^{PV/+}$ and especially the $Thrb^{PV/PV}$ genotypes and indicates cells with higher numbers of signals. **(B)** *y*-Axis indicates the number of signals per 100 cells observed at an intensity shown on the *x*-axis in arbitrary units (AU). This number was determined by dividing the number of signals observed by the total number of thyroid samples observed for each genotype. A shift upward indicates more signals of lesser intensity for $Thrb^{PV/+}$ and $Thrb^{PV/PV}$ genotypes, and a shift to the right indicates more signals of higher intensity for $Thrb^{PV/PV}$. **(C)** Representative thyroid areas (H&E stained) and individual thyrocyte nuclei selected from each genotype, DAPI nuclear stain with rhodamine-labelled telomere signals, **(i)** homozygous normal $Thrb^{+/+}$, **(ii)** heterozygous $Thrb^{PV/+}$ mutant, **(iii)** homozygous $Thrb^{PV/PV}$ mutant, shown as both 2D and 3D side nuclear images of telomere signals. Nuclei with more telomere signals are seen in nuclei of $Thrb^{PV/PV}$ thyrocytes. **(D)** Data from representative thyroid samples from mice of each genotype displaying signal intensity data. **(E)** Data from representative thyroid samples of mice for each genotype showing the number of signals per thyrocyte. Arrows indicate separate populations of cells with differing numbers of telomeres in the multipeaked $Thrb^{PV/PV}$ example.

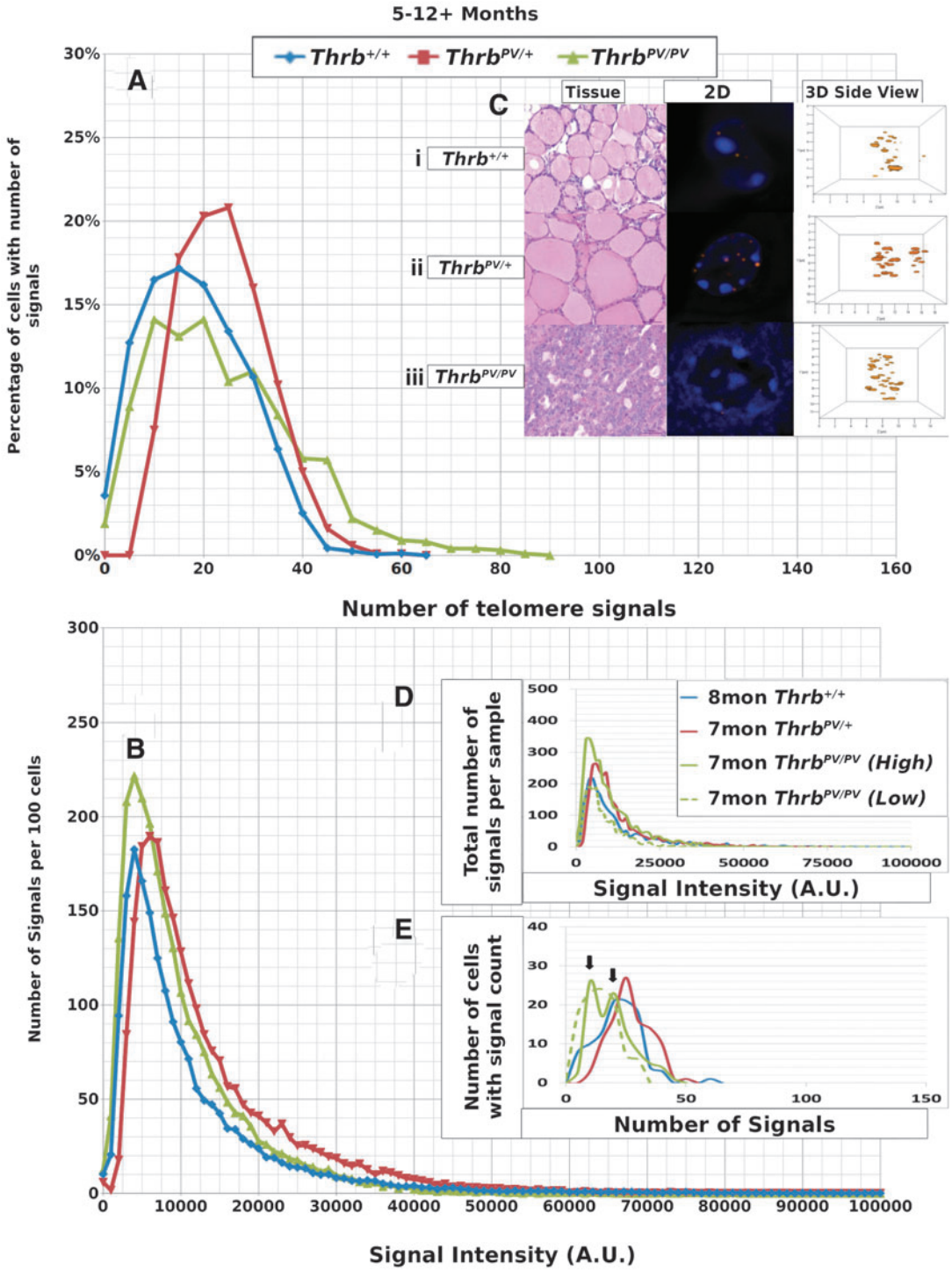

FIG. 3. Data for thyrocytes of mice sacrificed at 5–12+ months of age. **(A)** *y*-axis indicates the percentage of cells in the given genotypes that have the number of signals shown on the *x*-axis. **(B)** *y*-Axis indicates the number of signals per 100 thyrocytes observed at an intensity shown on the *x*-axis. In nuclei of $Thrb^{PV/PV}$ thyrocytes, a higher numbers of less intense telomere signals were observed, whereas in nuclei of the $Thrb^{PV/+}$ thyrocytes higher intensity signals were detected than in the nuclei of age-matched controls. **(C)** Representative H&E stained thyroid tissue sections and individual thyrocyte nuclei taken from each genotype, DAPI nuclear stain with rhodamine-labeled telomere signals, **(i)** homozygous normal $Thrb^{+/+}$, **(ii)** heterozygous $Thrb^{PV/+}$ mutant, **(iii)** homozygous $Thrb^{PV/PV}$ mutant, shown as both 2D and 3D side nuclear images of telomere signals. **(D)** Data from representative mouse thyroid samples of each genotype showing signal intensity versus number of signals. **(E)** Data from representative mouse thyroid samples of each genotype showing the number of signals per thyrocyte. Arrows highlight multiple $Thrb^{PV/PV}$ thyrocyte populations with specific signal counts.

length with age, terminal restriction fragment (TRF) failed to detect changes in telomere length in liver, testis, or kidney (44). Our 3D telomere FISH analysis revealed that, up to 12 months of age, the average telomere length in thyrocytes of wild type $Thrb^{+/+}$ mice with C57BL/J6 genetic background remained relatively stable (see B graphs of all figures). This allowed us to compare telomere profiles across different age groups and genotypes and demonstrate that homozygous $Thrb^{PV/PV}$ mice displayed the highest level of genomic instability followed by the $Thrb^{PV/+}$ genotype. Although we observed a higher number of shorter telomeres at early age in both $Thrb^{PV/PV}$ and the $Thrb^{PV/+}$ mutants, the $Thrb^{PV/PV}$ mice exclusively presented with various cell populations with different number of telomere signals (Fig. 2E) within the same animal. This suggests an early phase of telomere instability creating cells with various levels of genomic instability, including tetraploidy and aneuploidy. These alterations in 3D telomere profiles were apparent at very early ages and long before histological signs of FTC (13,15) were detectable in $Thrb^{PV/PV}$ mice. We previously described numerical (ranging from near diploid to near tetraploid) and structural chromosome aberration in thyroid cancer cell lines established from $Thrb^{PV/PV}$ mice (46). The presence of $Thrb^{PV/PV}$ thyrocyte populations with 40 or more telomere signals in several age groups is consistent with the notion that both aneuploid and/or tetraploid cells have tumorigenic properties (47–49). Aneuploidy is common in many human cancers (50,51) and serves as independent prognostic factor for clinical outcome of numerous cancer types, including differentiated and undifferentiated/anaplastic thyroid cancer (52–54).

In mammalian cells, the 3D nuclear position of telomeres is dependent on the cell cycle and cell type. In normal cells, telomeres are found in microterritories (35) and usually do not overlap or create aggregates (31). A telomeric disks is formed during G2 phase of the cell cycle (31) as determined by a substantially increase in the *a/c* ratio (30). Despite the thyroid hyperplasia in $Thrb^{PV/PV}$ mice (27), we failed to detect differences in the *a/c* ratio in thyroid epithelial cells of any mouse genotype studied. These results may in part be explained by the fact that, contrary to nuclei of cultured cells which are scanned entirely, it is difficult to assess the entire *a/c* ratio of telomere distribution in nuclei of tissue samples, since only the nuclear segment as presented within a particular tissue section can be analyzed. We have previously identified TA as a specific signature of tumor cells (19,31) which is independent of telomerase activity and telomere length (18). TA are telomere clusters with stronger intensity hybridization signals that cannot be further resolved as separate signals by conventional microscopy and likely represent end-to-end telomere fusions which cause breakage–fusion–bridge cycles (18,55,56), thus facilitating chromosomal rearrangements.

Telomere shortening was observed in human PTC (57). In our FTC mouse model, we detected the presence of shorter telomeres at a very early stage, suggesting that in FTC, as in other cancer types, alterations to the organization of the 3D nucleus promotes tumorigenesis as a result of chromosomal instability (58). Short and especially critically shortened telomeres represent telomere dysfunction and may form aggregates that likely are not classified as TA by the software, as their cumulative intensity falls below the threshold level for the fluorescence intensity of normal telomeres. In $Thrb^{PV/PV}$ mice, telomere instability is likely to be responsible for the appearance of several cell populations with deletions, gene amplifications, and/or nonreciprocal translocations we described earlier in cell lines derived from $Thrb^{PV/PV}$ tumors (46). Telomere-driven genomic instability in thyroid lesions was also detected by interphase FISH for cytogenetic subtyping of human thyroid lesions, revealing the presence of specific breakpoint chromosomal aberrations (37). Close proximity of telomere territories combined with altered telomere architecture can increase the risk of recombination especially in subtelomeric regions fuelling genomic instability (59). Our findings implicate telomere architectural changes to trigger early onset, continual, and competitive clonal selection of thyrocyte populations throughout follicular carcinogenesis.

Intriguingly, the 3D telomere profile of $Thrb^{PV/+}$ thyrocytes was different from wild type controls throughout all age groups. The majority of segmental nuclei of $Thrb^{PV/+}$ heterozygous thyrocytes showed increased average telomere numbers (Table 2), a higher percentage of nuclei with increased telomere signals (Figs. 2A, 3A), and longer telomeres (Figs. 2B, 3B). $Thrb^{PV/+}$ nuclei lacked the presence of multiple cell populations with different degrees of aneuploidy. Instead, they showed a homogeneous population of aneuploid nuclei with increased numbers of telomere signals (Figs. 2E, 3E). We interpret these observations as an underlying genomic instability in $Thrb^{PV/+}$ thyrocytes that requires additional stimuli for carcinoma initiation. Indeed, we demonstrated that elevated thyroid hormone levels (60), the lack of a wild type thyroid hormone receptor beta (TRβ) (13), and TSH levels that are elevated beyond a critical threshold level (61) can promote the initiation of FTC in $Thrb^{PV/+}$ thyrocytes. The exact mechanisms by which thyroid hormones and/or TSH can affect telomere architecture in $Thrb^{PV/+}$ thyrocytes remains to be elucidated.

In conclusion, 3D telomere FISH analysis was able to detect thyrocyte-specific alterations in telomere architecture starting as early as 1 month of age prior to histological signs of FTC in the $Thrb^{PV/PV}$ mouse model. In male and female $Thrb^{PV/PV}$ mice alike, FTC involved the dynamic selection of thyrocytes with shorter telomeres and aneuploid and tetraploid thyrocyte populations. These telomere changes were absent in heterozygous $Thrb^{PV/+}$ or control mice. Our findings confirm previous reports identifying 3D telomere FISH as an effective diagnostic tool for early detection of individual cancer cells, tumor subtypes, and suitable prognostic indicator of disease progression (24,25,31,62). Recently, we developed an automated 3D telomere scanning procedure capable of rapid imaging of telomere profiles from interphase nuclei, and specific TeloScan software was shown to identify individual tumor cells in large samples (63). This novel 3D telomere technique will make it feasible to test large numbers of human thyroid tissues in clinical screening rapidly.

Acknowledgments

S.H.K. and T.K. are both grateful for financial support from the Natural Sciences and Engineering Council of Canada (NSERC), the Manitoba Institute of Child Health (MICH), and the Department of Surgery Research Fund at the Faculty of Medicine, University of Manitoba. L.W. is the recipient of a Manitoba Health Research Council (MHRC) fellowship and S.M. is supported by the Canadian Institutes of Health

Research (CIHR). The authors thank Ms. Mary Cheang for statistical analysis of the data.

Author Disclosure Statement

No competing financial interests exist.

References

1. National Cancer Institute 2012 SEER stat fact sheets: thyroid cancer. Available online at http://seer.cancer.gov/statfacts/html/thyro.html
2. Bhaijee F, Nikiforov YE 2011 Molecular analysis of thyroid tumors. Endocr Pathol **22:**126–133.
3. Nishisho I, Nakamura Y, Miyoshi Y 1991 Mutations of chromosome 5q21 genes in FAP and colorectal cancer patients. Science **253:**665–669.
4. Liaw D, Marsh D, Li J, Dahia P, Wang S 1997 Germline mutations of the PTEN gene in Cowden disease, an inherited breast and thyroid cancer syndrome. Nature **16:**64–67.
5. Kirschner LS, Carney JA, Pack SD, Taymans SE, Giatzakis C, Cho YS, Cho-Chung YS, Stratakis CA 2000 Mutations of the gene encoding the protein kinase A type I-alpha regulatory subunit in patients with the Carney complex. Nat Genet **26:**89–92.
6. Blumenthal GM, Dennis PA 2008 PTEN hamartoma tumor syndromes. Eur J Hum Genet **16:**1289–1300.
7. Kondo T, Ezzat S, Asa SL 2006 Pathogenetic mechanisms in thyroid follicular-cell neoplasia. Nat Rev Cancer **6:**292–306.
8. Yeager N, Klein-Szanto A, Kimura S, Di Cristofano A 2007 Pten loss in the mouse thyroid causes goiter and follicular adenomas: insights into thyroid function and Cowden disease pathogenesis. Cancer Res **67:**959–966.
9. Nikiforova MN 2003 RAS point mutations and PAX8-PPARgamma rearrangement in thyroid tumors: evidence for distinct molecular pathways in thyroid follicular carcinoma. J Clin Endocrinol Metab **88:**2318–2326.
10. Kroll TG 2000 PAX8-PPARgamma 1 fusion in oncogene human thyroid carcinoma. Science **289:**1357–1360.
11. Kato Y, Ying H, Zhao L, Furuya F, Araki O, Willingham MC, Cheng SY 2006 PPARgamma insufficiency promotes follicular thyroid carcinogenesis via activation of the nuclear factor-kappaB signaling pathway. Oncogene **25:**2736–2747.
12. Puzianowska-Kuznicka M, Krystyniak A, Madej A, Cheng S-Y, Nauman J 2002 Functionally impaired TR mutants are present in thyroid papillary cancer. J Clin Endocrinol Metab **87:**1120–1128.
13. Kato Y, Ying H, Willingham MC, Cheng S-Y 2004 A tumor suppressor role for thyroid hormone beta receptor in a mouse model of thyroid carcinogenesis. Endocrinology **145:**4430–4438.
14. Araki O, Ying H, Furuya F 2005 Thyroid hormone receptor beta mutants: dominant negative regulators of peroxisome proliferator-activated receptor gamma action. Proc Natl Acad Sci USA **102:**16251–16256.
15. Suzuki H, Willingham M, Cheng S 2002 Mice with a mutation in the thyroid hormone receptor beta gene spontaneously develop thyroid carcinoma: a mouse model of thyroid carcinogenesis. Thyroid **12:**963–969.
16. Ferrara AM, Onigata K, Ercan O, Woodhead H, Weiss RE, Refetoff S 2012 Homozygous thyroid hormone receptor β-gene mutations in resistance to thyroid hormone: three new cases and review of the literature. J Clin Endocrinol Metab **97:**1328–1336.
17. De Lange T 2005 Shelterin: the protein complex that shapes and safeguards human telomeres. Genes Dev **19:**2100–2110.
18. Louis SF, Vermolen BJ, Garini Y, Young IT, Guffei A, Lichtensztejn Z, Kuttler F, Chuang TC, Moshir S, Mougey V, Chuang AY, Kerr PD, Fest T, Boukamp P, Mai S 2005 c-Myc induces chromosomal rearrangements through telomere and chromosome remodeling in the interphase nucleus. Proc Natl Acad Sci USA **102:**9613–9618.
19. Mai S, Garini Y 2006 The significance of telomeric aggregates in the interphase nuclei of tumor cells. J Cell Biochem **97:**904–915.
20. Desmaze C, Soria J-C, Freulet-Marrière M-A, Mathieu N, Sabatier L 2003 Telomere-driven genomic instability in cancer cells. Cancer Lett **194:**173–182.
21. Gollin SM 2008 Mechanisms leading to nonrandom, nonhomologous chromosomal translocations in leukemia. Semin Cancer Biol **17:**74–79.
22. Kuttler F, Mai S 2007 Formation of non-random extrachromosomal elements during development, differentiation and oncogenesis. Semin Cancer Biol **17:**56–64.
23. Mai S 2010 Initiation of telomere-mediated chromosomal rearrangements in cancer. J Cell Biochem **109:**1095–1102.
24. Knecht H, Kongruttanachok N, Sawan B, Turcotte E, Lichtensztejn Z, Lichtensztejn D, Mai S 2012 Three-dimensional telomere signatures of Hodgkin- and Reed-Sternberg cells at diagnosis identify patients with poor response to conventional chemotherapy. Transl Oncol **5:**269–277.
25. Gadji M, Fortin D, Tsanaclis A 2010 Three-dimensional nuclear telomere architecture is associated with differential time to progression and overall survival in glioblastoma patients. Neoplasia **12:**183–191.
26. Gadji M, Adebayo Awe J, Rodrigues P, Kumar R, Houston DS, Klewes L, Dièye TN, Rego EM, Passetto RF, de Oliveira FM, Mai S 2012 Profiling three-dimensional nuclear telomeric architecture of myelodysplastic syndromes and acute myeloid leukemia defines patient subgroups. Clin Cancer Res **18:**3293–3304.
27. Kaneshige M, Kaneshige K, Zhu X, Dace a, Garrett L, Carter TA, Kazlauskaite R, Pankratz DG, Wynshaw-Boris A, Refetoff S, Weintraub B, Willingham MC, Barlow C, Cheng S 2000 Mice with a targeted mutation in the thyroid hormone beta receptor gene exhibit impaired growth and resistance to thyroid hormone. Proc Natl Acad Sci USA **97:**13209–13214.
28. Hopman AH, Van Hooren E, Van De Kaa CA, Vooijs PG, Ramaekers FC 1991 Detection of numerical chromosome aberrations using in situ hybridization in paraffin sections of routinely processed bladder cancers. Mod Pathol **4:**503–513.
29. Schaefer LH, Schuster D, Herz H 2001 Generalized approach for accelerated maximum likelihood based image restoration applied to three-dimensional fluorescence microscopy. J Microscopy **204:**99–107.
30. Vermolen BJ, Garini Y, Mai S, Mougey V, Fest T, Chuang TC, Wark L, Young IT 2005 Characterizing the three-dimensional organization of telomeres. Cytometry **6:**144–150.
31. Chuang T, Moshir S, Garini Y, Ya- A, Chuang C, Young IT, Vermolen B, van den Doel R, Mougey V, Perrin M, Braun M, Kerr PD, Fest T, Boukamp P, Mai S 2004 The three-dimensional organization of telomeres in the nucleus of mammalian cells. BMC Biol **2:**1–8.
32. Poon SS, Martens UM, Ward RK, Lansdorp PM 1999 Telomere length measurements using digital fluorescence microscopy. Cytometry **36:**267–278.
33. Nagele RG, Velasco a Q, Anderson WJ, McMahon DJ, Thomson Z, Fazekas J, Wind K, Lee H 2001 Telomere as-

sociations in interphase nuclei: possible role in maintenance of interphase chromosome topology. J Cell Sci **114:**377–388.
34. Weierich C, Brero A, Stein S, Von Hase J, Cremer C, Cremer T, Solovei I 2003 Three-dimensional arrangements of centromeres and telomeres in nuclei of human and murine lymphocytes. Chromosome Res **11:**485–502.
35. De Vos WH, Hoebe R a, Joss GH, Haffmans W, Baatout S, Van Oostveldt P, Manders EM 2009 Controlled light exposure microscopy reveals dynamic telomere microterritories throughout the cell cycle. Cytometry A **75:**428–439.
36. Caporali A, Wark L, Vermolen BJ, Garini Y, Mai S 2007 Telomeric aggregates and end-to-end chromosomal fusions require myc box II. Oncogene **26:**1398–1406.
37. Drieschner N, Rippe V, Laabs A, Dittberner L, Nimzyk R, Junker K, Rommel B, Kiefer Y, Belge G, Bullerdiek J, Sendt W 2011 Interphase fluorescence in situ hybridization analysis detects a much higher rate of thyroid tumors with clonal cytogenetic deviations of the main cytogenetic subgroups than conventional cytogenetics. Cancer Genet **204:**366–374.
38. Meeker AK, Hicks JL, Iacobuzio-Donahue CA, Montgomery EA, Westra WH, Chan TY, Ronnett BM, De Marzo AM 2004 Telomere length abnormalities occur early in the initiation of epithelial carcinogenesis. Clin Cancer Res **10:**3317–3326.
39. Meeker AK, Hicks JL, Gabrielson E, Strauss WM, De Marzo AM, Argani P 2004 Telomere shortening occurs in subsets of normal breast epithelium as well as *in situ* and invasive carcinoma. Am J Pathol **164:**925–935.
40. Meeker AK, Hicks JL, Platz EA, March GE, Bennett CJ, Delannoy MJ, De Marzo AM 2002 Telomere shortening is an early somatic DNA alteration in human prostate tumorigenesis. Cancer Res **62:**6405–6409.
41. Van Heek NT, Meeker AK, Kern SE, Yeo CJ, Lillemoe KD, Cameron JL, Offerhaus GJ, Hicks JL, Wilentz RE, Goggins MG, De Marzo AM, Hruban RH, Maitra A Telomere shortening is nearly universal in pancreatic intraepithelial neoplasia. Am J Pathol **161:**1541–1547.
42. Cesare AJ, Reddel RR 2010 Alternative lengthening of telomeres: models, mechanisms and implications. Nat Rev Genet **11:**319–330.
43. Shay JW, Wright WE 2011 Role of telomeres and telomerase in cancer. Semin Cancer Biol **21:**349–353.
44. Coviello-McLaughlin GM, Prowse KR 1997 Telomere length regulation during postnatal development and ageing in Mus spretus. Nucleic Acids Res **25:**3051–3058.
45. Rudolph KL, Chang S, Lee HW, Blasco M, Gottlieb GJ, Greider C, DePinho RA 1999 Longevity, stress response, and cancer in aging telomerase-deficient mice. Cell **96:**701–712.
46. Zimonjic DB, Kato Y, Ying H, Popescu NC, Cheng S-Y 2005 Chromosomal aberrations in cell lines derived from thyroid tumors spontaneously developed in TRbetaPV/PV mice. Cancer Genet Cytogenet **161:**104–109.
47. Fujiwara T, Bandi M, Nitta M, Ivanova EV, Bronson RT, Pellman D 2005 Cytokinesis failure generating tetraploids promotes tumorigenesis in p53-null cells. Nature **437:**1043–1047.
48. Ganem NJ, Storchova Z, Pellman D 2007 Tetraploidy, aneuploidy and cancer. Curr Opin Genet Dev **17:**157–162.
49. Davoli T, De Lange T 2012 Telomere-driven tetraploidization occurs in human cells undergoing crisis and promotes transformation of mouse cells. Cancer Cell **21:**765–776.
50. Gordon DJ, Resio B, Pellman D 2012 Causes and consequences of aneuploidy in cancer. Nat Rev Genet **13:**189–203.
51. Jonsdottir AB, Stefansson OA, Bjornsson J, Jonasson JG, Ogmundsdottir HM, Eyfjord JE 2012 Tetraploidy in BRCA2 breast tumours. Eur J Cancer **48:**305–310.
52. Sturgis CD, Caraway NP, Johnston DA, Sherman SI, Kidd L, Katz RL 1999 Image analysis of papillary thyroid carcinoma fine-needle aspirates: significant association between aneuploidy and death from disease. Cancer **87:**155–160.
53. Miura D, Wada N, Chin K, Magrane GG, Wong M, Duh Q-Y, Clark OH 2003 Anaplastic thyroid cancer: cytogenetic patterns by comparative genomic hybridization. Thyroid **13:**283–290.
54. Pinto AE, Silva G, Banito ANA, Leite V, Soares J 2008 Aneuploidy and high S-phase as biomarkers of poor clinical outcome in poorly differentiated and anaplastic thyroid carcinoma. Oncol Rep **20:**913–919.
55. McClintock B 1941 The stability of broken ends of chromosomes in Zea Mays. Genetics **26:**234–282.
56. Mueller J 1938 A synthetic medium for the cultivation of *C. diphtheriae*. J Baceteriol **36:**499–515.
57. Capezzone M, Cantara S, Marchisotta S, Busonero G, Formichi C, Benigni M, Capuano S, Toti P, Pazaitou-Panayiotou K, Caruso G, Carli AF, Palummo N, Pacini F 2011 Telomere length in neoplastic and nonneoplastic tissues of patients with familial and sporadic papillary thyroid cancer. J Clin Endocrinol Metab **96:**1852–1856.
58. Maicher A, Kastner L, Dees M, Luke B 2012 Deregulated telomere transcription causes replication-dependent telomere shortening and promotes cellular senescence. Nucleic Acid Res **40:**6649–6659.
59. Linardopoulou E, Williams E, Fan Y 2005 Human subtelomeres are hot spots of interchromosomal recombination and segmental duplication. Nature **437:**94–100.
60. Lu C, Zhu X, Willingham MC, Cheng S-Y 2012 Activation of tumor cell proliferation by thyroid hormone in a mouse model of follicular thyroid carcinoma. Oncogene **31:**2007–2016.
61. Zhao L, Zhu X, Won Park J, Fozzatti L, Willingham M, Cheng S 2012 Role of TSH in the spontaneous development of asymmetrical thyroid carcinoma in mice with a targeted mutation in a single allele of the thyroid hormone-β receptor. Endocrinology **153:**5090–5100.
62. Kuzyk A, Mai S 2012 Selected telomere length changes and aberrant three-dimensional nuclear telomere organization during fast-onset mouse plasmacytomas. Neoplasia **14:**344–351.
63. Klewes L, Höbsch C, Katzir N, Rourke D, Garini Y, Mai S 2011 Novel automated three-dimensional genome scanning based on the nuclear architecture of telomeres. Cytometry A **79:**159–166.

Address correspondence to:
Thomas Klonisch, MD, PhD
Dept. of Human Anatomy and Cell Science, Faculty of Medicine
University of Manitoba
130 Basic Medical Sciences
130-745 Bannatyne Avenue
Winnipeg, MB, R3E 0J9
Canada

E-mail: thomas.klonisch@med.umanitoba.ca